Chapter 4

Multiwavelet Characteristics

4.1 Multiwavelets: Examples

Several balanced multiwavelets with diverse characteristics are described in the literature [10, 11, 19, 26, 33]. In this chapter we analyze the characteristics of five balanced multiwavelets and their effect on image compression performance. To underscore the importance of balancing, we also present the analysis for two unbalanced multiwavelets. Table 4.1 lists the multiwavelets analyzed in this thesis and introduces a shorthand notation for brevity.

SA_4^u [26] and Ort_4^u [33] are unbalanced multiwavelets. When the pre-, post-filtering operations described in [26, 33] are absorbed into the filter bank coefficients, we get the corresponding second order balanced multiwavelets, SA_4^b [26] and Ort_4^b [33]. Bmw_8 and Bmw_{12} are balanced multiwavelets with balancing order 2 and 3, respectively [11]. The Bmw_S multiwavelet is balanced to order 2 and has symmetric (i.e. linear-phase) filters in its time-varying filter bank [19].

Table 4.1: Notation for multiwavelets discussed in this thesis

Notation	Description
SA_4^u	Symmetric-Antisymmetric multiwavelet, with 8-tap filters, without pre and post-processing (unbalanced) [26]
Ort_4^u	Orthogonal multiwavelet, with 8-tap filters, without pre and post-processing (unbalanced)[33]
SA_4^b	SA_4^u modified by pre and post-processing (balanced) [26]
Ort_4^b	Ort_4^u modified by pre and post-processing (balanced) [33]
Bmw_8	The balanced 8-tap multiwavelet in [11]
Bmw_S	The balanced multiwavelet based on symmetric filters in [19]
Bmw_{12}	The balanced 12-tap multiwavelet in [11]

4.2 Filter Bank Characteristics

The balancing order largely determines the energy compaction capability of the multiwavelet transform and is therefore the primary determinant of the error in the compressed image. On the basis of the balancing order, we expect the balanced multiwavelets to outperform the unbalanced multiwavelets. Amongst the balanced multiwavelets we expect the Bmw_{12} multiwavelet that has the highest balancing order to give the best results.

However, the balancing order is not indicative of the error distribution pattern in the reconstructed image. In fact, the multiwavelet characteristics that affect the error distribution include shift-variance, magnitude and phase characteristics, symmetry of bases and compactly supported filters. In the following subsections, we perform a comparative analysis of these characteristics for the first time. Our goal is to better understand those multiwavelet characteristics that are most important to image compression performance.

4.2.1 Behavior under Shift-variance

To fully understand the behavior of an iterated multiwavelet filter bank, we need to study its behavior under integer shifts of its filters[19]. For $r = 2$ the multiwavelet filter bank generates one set of basis functions for even shifts and another set of basis functions for odd shifts. Let $\phi_{i,0}(t)$ and $\psi_{i,0}(t)$ $(i = 0, 1)$ represent the scaling and wavelet functions for a zero shift. Let $\phi_{i,1}(t)$ and $\psi_{i,1}(t)$ ($i = 0, 1$ for $r = 2$) represent the scaling and wavelet functions for unity shift. (We do not need to consider any other shifts since all even shifts correspond to $\phi_{i,0}(t)$, $\psi_{i,0}(t)$ and all odd shifts correspond to $\phi_{i,1}(t)$, $\psi_{i,1}(t)$). Similar to a scalar wavelet filter bank (where an integer shift of its filters results in the same shift of $\phi(t)$ and $\psi(t)$), it is desired that the multiwavelet filter bank be invariant under integer shifts, i.e. $\phi_{i,1}(t)$ and $\psi_{i,1}(t)$ should be shifted versions of $\phi_{i,0}(t)$ and $\psi_{i,0}(t)$.

Unbalanced multiwavelet filter banks are typically shift-variant [19]. In Figures 4.1 and 4.2 the SA_4^u and Ort_4^u basis functions $\phi_{i,1}(t)$ and $\psi_{i,1}(t)$ are not shifted versions of $\phi_{i,0}(t)$ and $\psi_{i,0}(t)$; moreover, they are not smooth.

These multiwavelets can be balanced by appropriate pre-filters [26, 33]. After the pre- and post-processing, we achieve the SA_4^b and Ort_4^b multiwavelets that have smooth and shift-invariant bases as shown in Figures 4.3 and 4.4.

However, in general, balancing does not guarantee shift-invariance. Figure 4.5 shows that the Bmw_8 balanced multiwavelet has smooth basis functions under odd integer shifts ($\phi_{i,1}(t)$ and $\psi_{i,1}(t)$) but they are not shifted versions of $\phi_{i,0}(t)$ and $\psi_{i,0}(t)$.

The shifted basis functions of Bmw_s are shown in Figure 4.6. Its basis functions $\phi_{i,1}(t)$ and $\psi_{i,1}(t)$ are smooth and the same as the flipped and shifted functions $\phi_{i,0}(t)$ and $\psi_{i,0}(t)$. Figure 4.7 shows that the Bmw_{12} multiwavelet is shift-invariant and smooth.

In short, balanced multiwavelets have smooth basis functions while typically, unbalanced multiwavelets have irregular basis functions. Further, not all balanced multiwavelet filter banks are invariant to integer shifts.

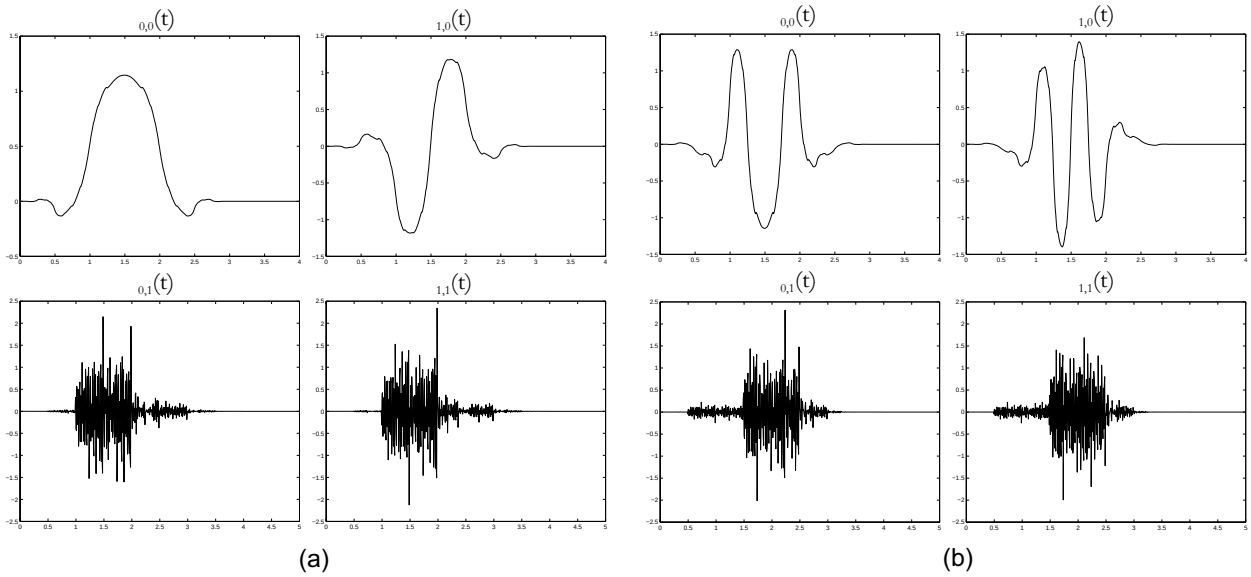

Figure 4.1: SA_4^u bases for even and odd integer shifts (a) scaling functions, (b) wavelet functions.

Quantization is a non-linear processing technique; it introduces frequency and phase distortion in the form of integer shifts in the wavelet-transformed image. For a shift-variant filter bank, the synthesis bank reconstructs the output with different bases depending on the phase distortion due to quantization. So, we expect shift-variance to degrade image compression performance; results in Chapter 5 support this statement. We also expect the non-smooth basis functions of the unbalanced multiwavelets to generate poorer results than the smooth basis functions of the balanced multiwavelets.

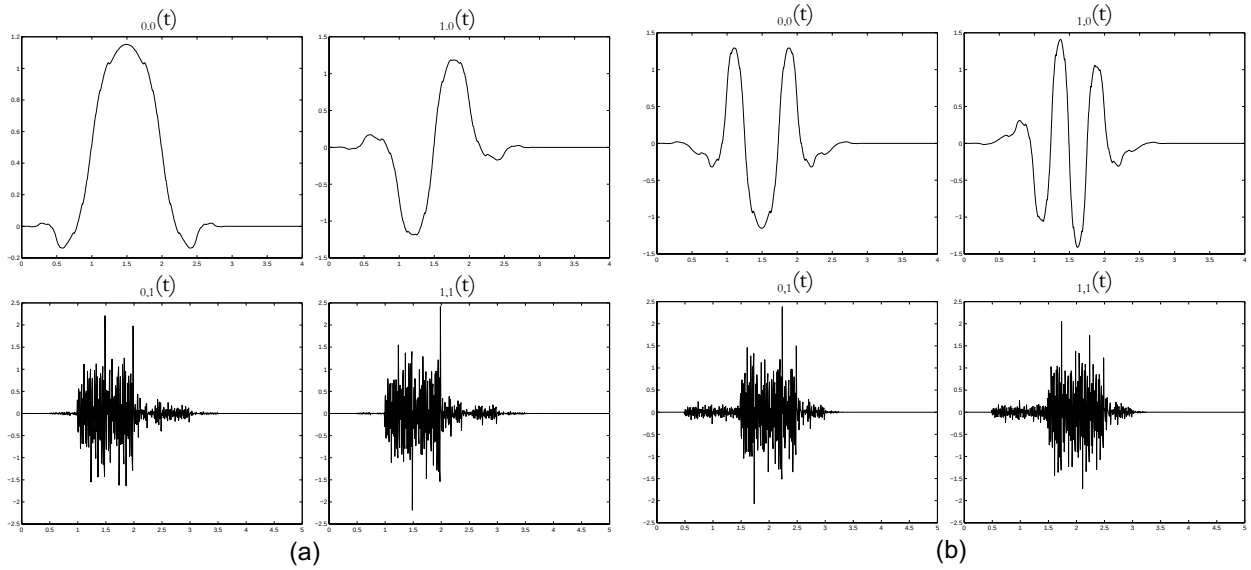

Figure 4.2: $\mathrm{Ort}_4^{\mathsf{u}}$ bases for even and odd integer shifts (a) scaling functions, (b) wavelet functions.

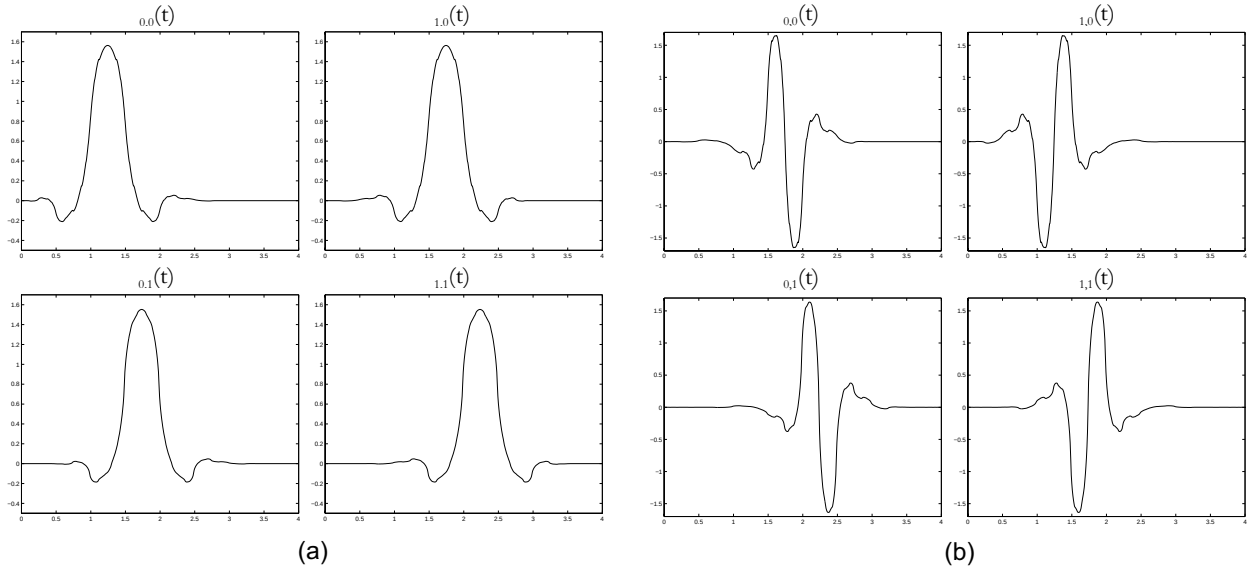

Figure 4.3: $\mathrm{SA}_4^{\mathsf{b}}$ bases for even and odd integer shifts (a) scaling functions, (b) wavelet functions.

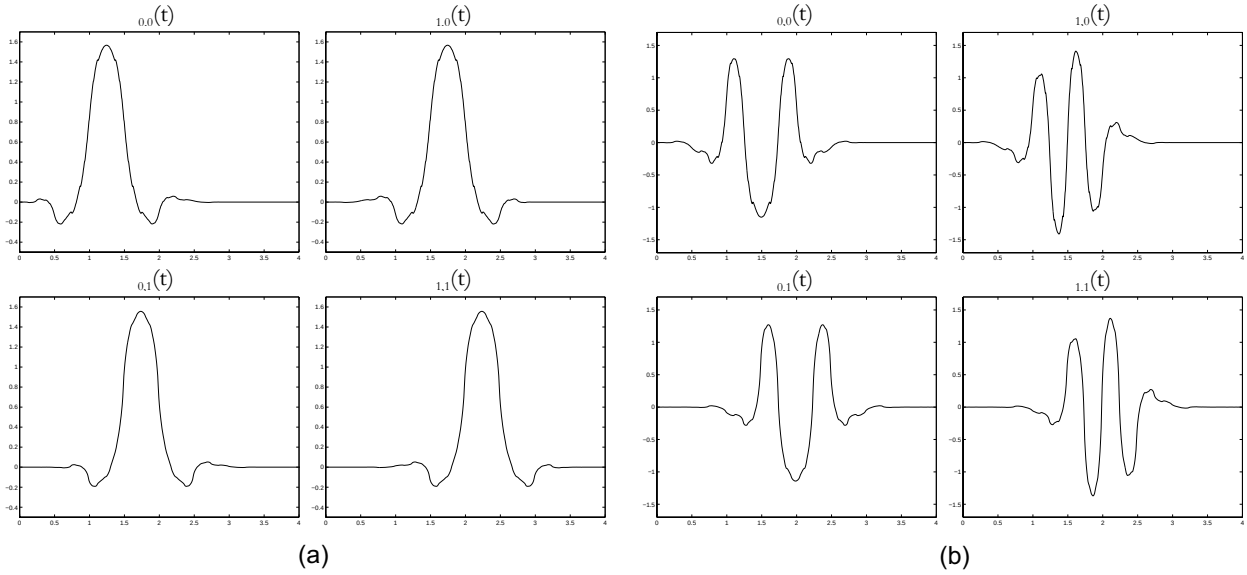

Figure 4.4: $\mathrm{Ort}_4^{\flat}$ bases for even and odd integer shifts (a) scaling functions, (b) wavelet functions.

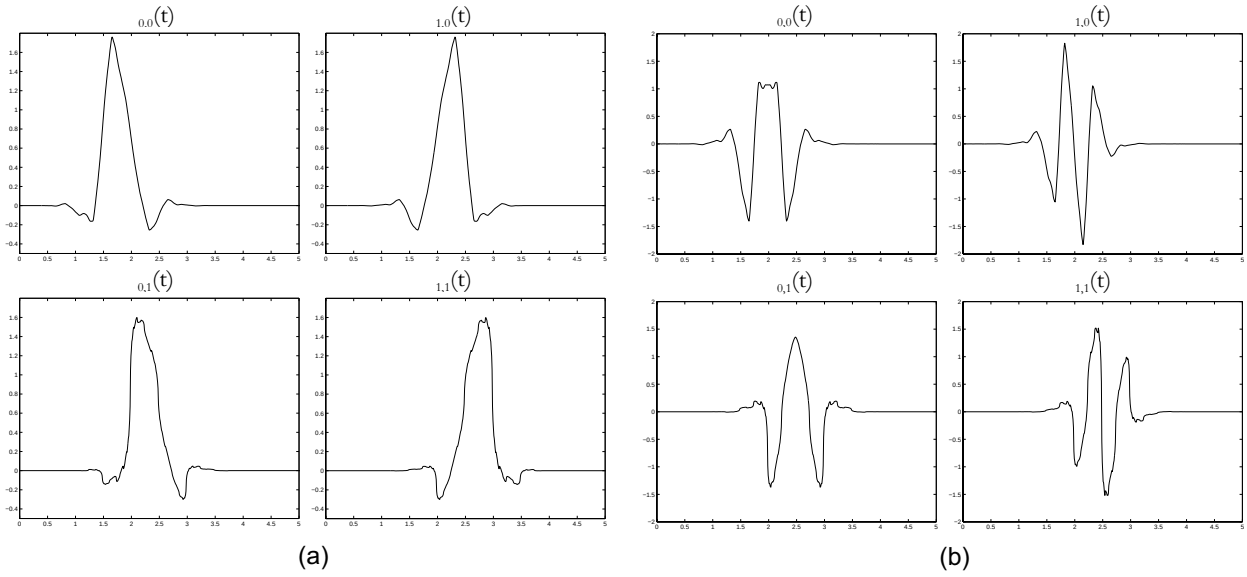

Figure 4.5: Bmw_8 bases for even and odd integer shifts (a) scaling functions, (b) wavelet functions.

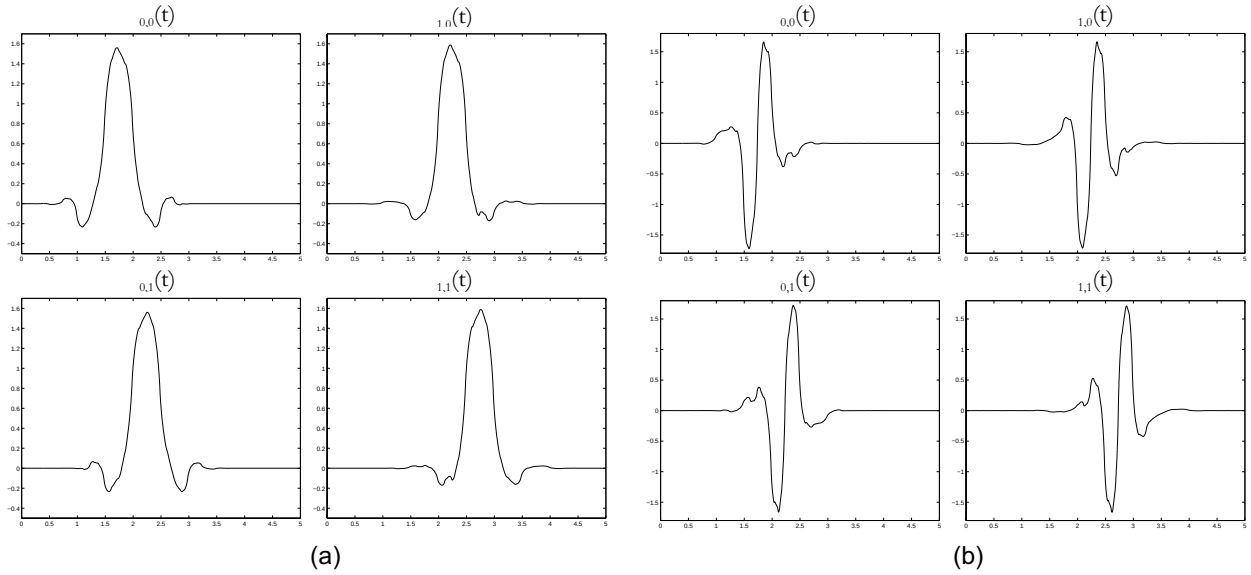

Figure 4.6: Bmw$_S$ bases for integer even and odd shifts (a) scaling functions, (b) wavelet functions.

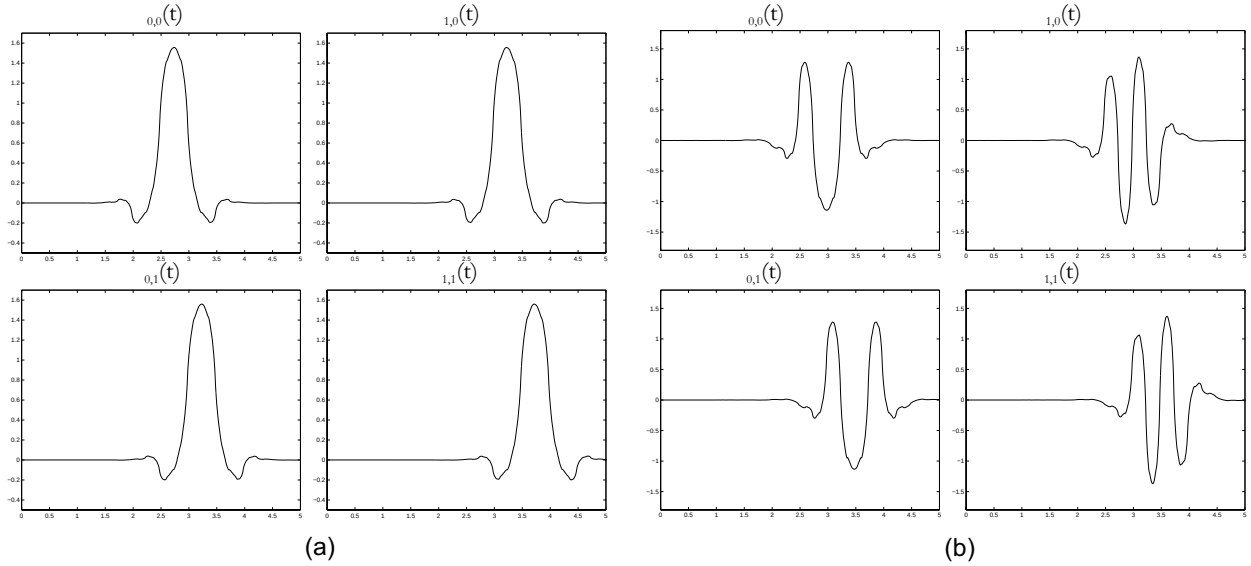

Figure 4.7: Bmw$_{12}$ bases for even and odd integer shifts (a) scaling functions, (b) wavelet functions.

4.2.2 Magnitude Spectrum Characteristics

The magnitude response characteristics of the filters in the multiwavelet filter bank affect the subjective image quality. Scalar wavelet filter bank characteristics that are good for image compression have been discussed in [23]. We extend this analysis to the multiwavelet filter banks. Ideally, the lowpass and highpass filters should decay smoothly to zero. Moreover, the lowpass branch filters should capture all of the dc energy and the highpass branch filters should have zero magnitude response at dc ($\omega = 0$ or equivalently $f = 0$). If the response of the bandpass/highpass filters is non-zero at dc, then under severe quantization of the high frequency coefficients, the checkerboard artifact appears in the reconstructed image [23]. Conversely, if the lowpass filters are not zero at the highest frequency ($\omega = \pi$ or equivalently $f = 0.5$), tiling (also called blocking) artifacts occur in the compressed image [23].

Figures 4.8–4.14 depict the magnitude spectra (computed using the FFT) of the four filters for each of the multiwavelet filter banks under consideration. $\mathrm{SA}_4^{\mathsf{u}}$ (Figure 4.8) and $\mathrm{Ort}_4^{\mathsf{u}}$ (Figure 4.9) do not even come close to the ideal magnitude response characteristics; they do not even have lowpass filters! Quantization will most likely give rise to checkerboard artifacts in images compressed using $\mathrm{SA}_4^{\mathsf{u}}$ and $\mathrm{Ort}_4^{\mathsf{u}}$.

All balanced multiwavelets come close to approximating the desired magnitude characteristics. Figure 4.10 shows that $\mathrm{SA}_4^{\mathsf{b}}$ has the best magnitude response characteristics amongst the remaining multiwavelets. Its lowpass and highpass branch filters decay smoothly and exactly to zero at $f = 0.5$ and $f = 0$, respectively. The $\mathrm{Ort}_4^{\mathsf{b}}$ multiwavelet has smoothly decaying lowpass filter responses. Its highpass filter g_1 has a low energy side-lobe at lower frequencies. Bmw_8 has lowpass filters that do not decay to zero at $f = 0.5$ (Figure 4.12), so we expect tiling artifacts with Bmw_8. Figure 4.13 shows that $\mathrm{Bmw}_{\mathsf{S}}$ has one lowpass branch filter (h_0) with a low-energy side-lobe. At low bit rates, we expect the truncation of this energy to produce the tiling artifact. For Bmw_{12}, the lowpass magnitude response at $f = 0.5$ is a small non-zero value as seen in Figure 4.14. Again, we expect to see mild tiling in images compressed with Bmw_{12}.

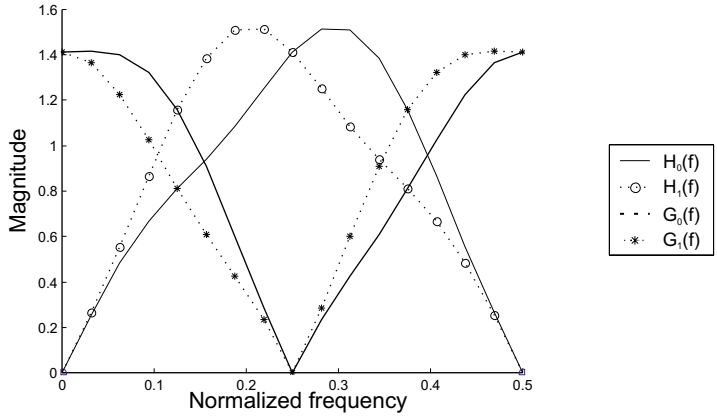

Figure 4.8: Magnitude characteristics of SA_4^u filter bank

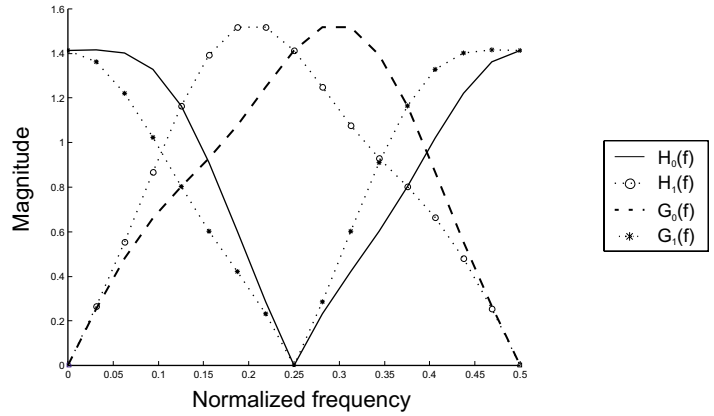

Figure 4.9: Magnitude characteristics of Ort_4^u filters.

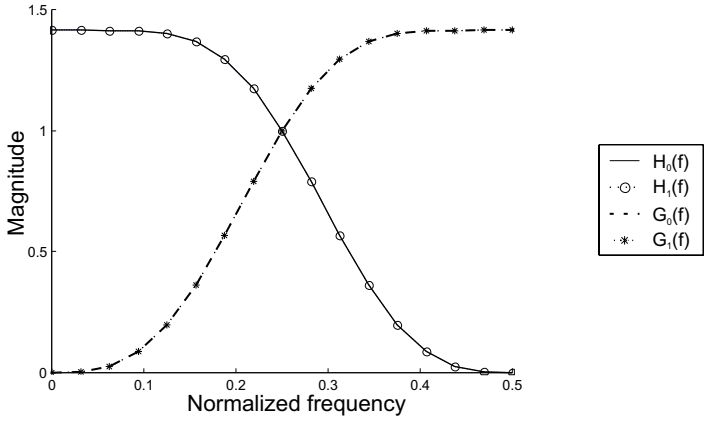

Figure 4.10: Magnitude characteristics of SA_4^b filters.

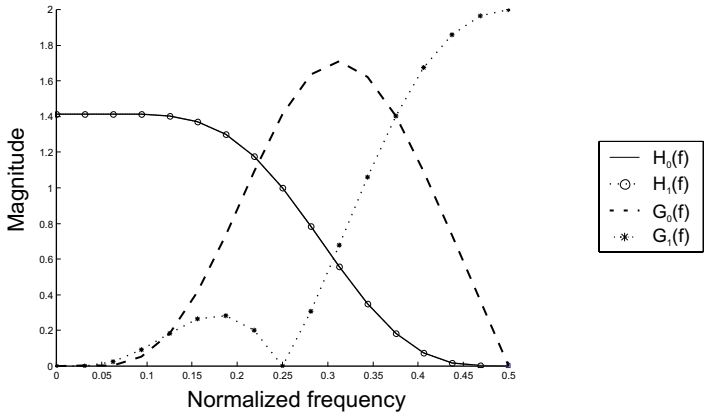

Figure 4.11: Magnitude characteristics of Ort_4^b filters.

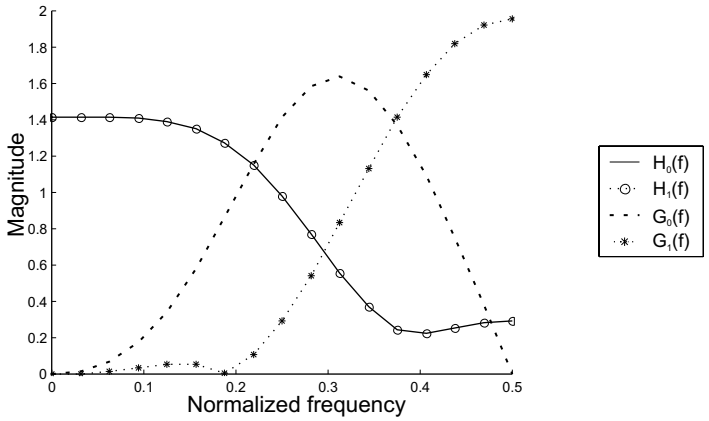

Figure 4.12: Magnitude characteristics of Bmw_8 filters.

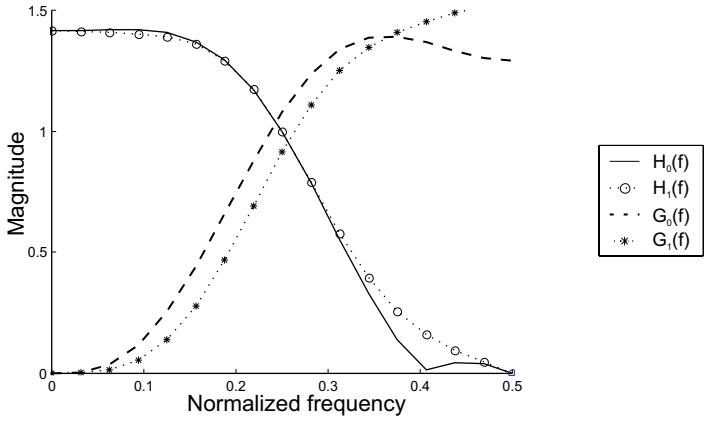

Figure 4.13: Magnitude characteristics of Bmw_S filters.

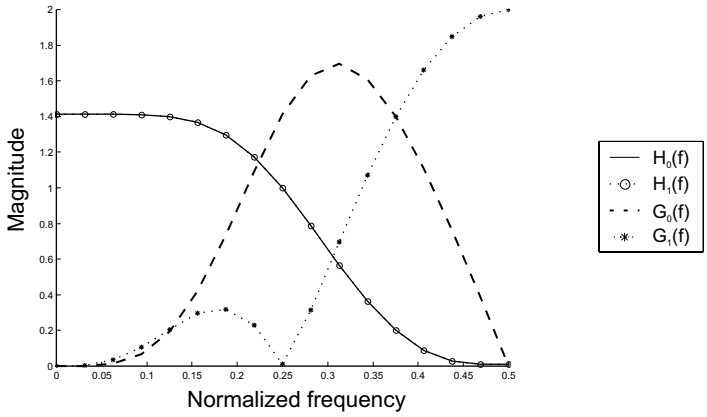

Figure 4.14: Magnitude characteristics of Bmw_{12} filters.

4.2.3 Group Delay Characteristics

For the balanced multiwavelets, in light of iteratively decomposing the shuffled low frequency band, the group delay and phase characteristics of the lowpass filters become important. (We do not analyze the group delay characteristics for the unbalanced multiwavelets since the lowpass branch outputs are not interleaved due to their dissimilar spectral behavior).

Figure 4.15 shows the output at every stage of the lowpass branch of the balanced multiwavelet filter bank for an arbitrary input. Suppose that h_0 introduces a group delay of 2 samples more than h_1. Then, the output of h_0 lags the output of h_1 by 2 samples. As seen in the figure, the downsampler outputs maintain the group delay difference. The output samples from h_0 and h_1 correspond to alternate samples in the interleaved output. The interleaving operation is equivalent to upsampling the downsampler output from the h_0-branch by two and adding it to the corresponding upsampled signal from the h_1-branch delayed by one sample. Thus, samples from one branch are always ahead of the other in the interleaved output. As expected, the interleaved output looks like an approximation of the input.

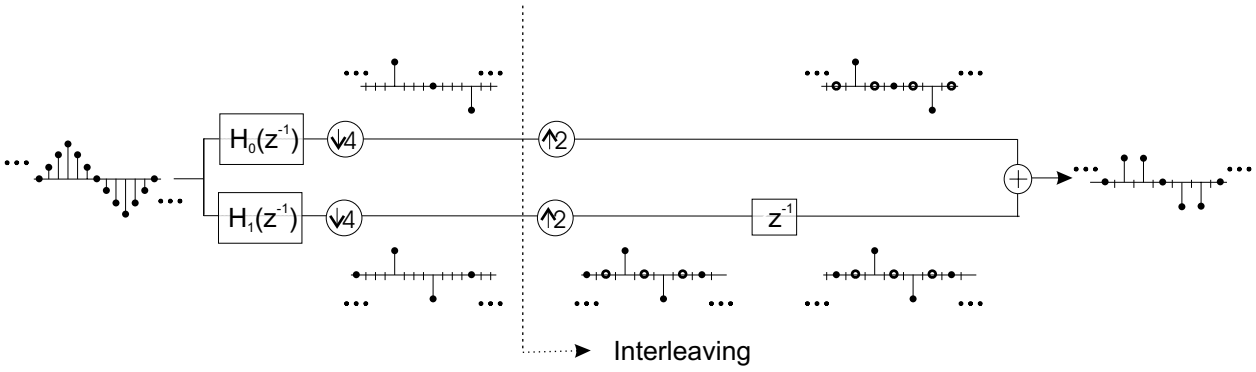

Figure 4.15: Lowpass branch output of a balanced multiwavelet with a group delay difference of 2.

If a group-delay difference of two (between h_0 and h_1) is absent, the interleaved samples do not have the correct phase; this distorts the phase of the lowpass output. In such a case, the wavelet coefficients fail to align properly across scales in a multilevel decomposition. This

affects the spatial correlation and the significance tree prediction and thus, compression performance is degraded.

Figures 4.16–4.20 show the group-delay plots for h_0 and h_1 for the five balanced multiwavelets. The group delay condition is perfectly satisfied only by the linear phase FIR filters in the $\mathrm{Bmw}_{\mathsf{S}}$ filter bank. For $\mathrm{SA}_4^{\mathsf{b}}$, $\mathrm{Ort}_4^{\mathsf{b}}$ and Bmw_{12}, at low and mid-range frequencies, the group delay difference is approximately equal to two but considerable distortion occurs at high frequencies. The Bmw_8 balanced multiwavelet fails to satisfy the group delay condition for frequencies $f > 0.3$ (Figure 4.18). We expect the non-ideal group delay characteristics to affect the Bmw_8 multiwavelet the most.

We expect that this group delay characteristic has less impact on compression performance than the shift-variance and magnitude characteristics because the lowpass filter magnitude response is small over the frequencies where the phase distortion occurs. Moreover, most images contain relatively little energy at high frequencies.

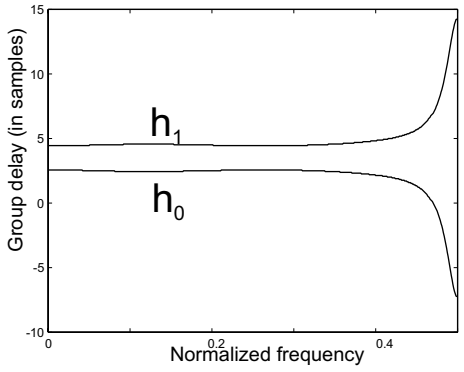

Figure 4.16: Group delay characteristics of $\mathrm{SA}_4^{\mathsf{b}}$ lowpass filters.

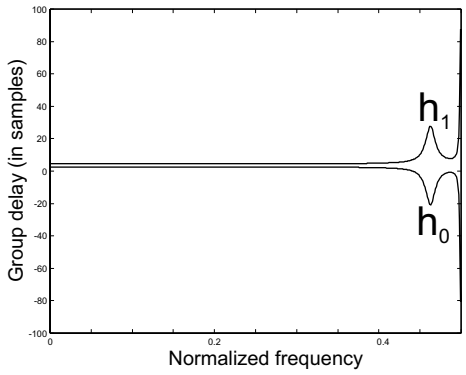

Figure 4.17: Group delay characteristics of $\mathrm{Ort}_4^{\mathsf{b}}$ lowpass filters.

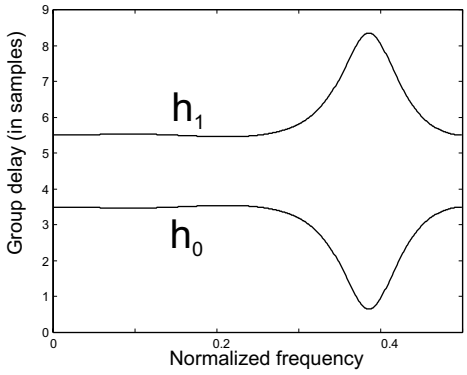

Figure 4.18: Group delay characteristics of Bmw_8 lowpass filters.

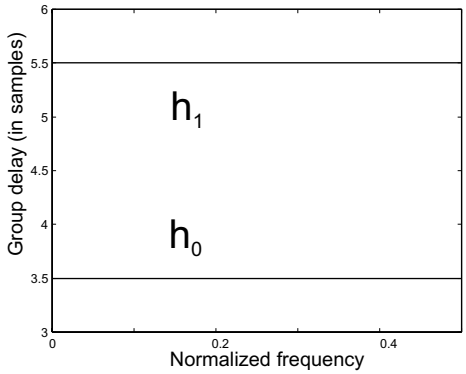

Figure 4.19: Group delay characteristics of $\mathrm{Bmw}_{\mathsf{S}}$ lowpass filters.

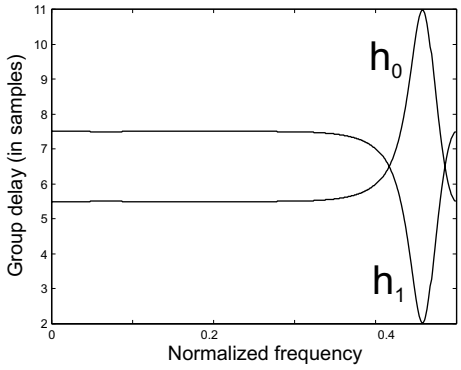

Figure 4.20: Group delay characteristics of Bmw_{12} lowpass filters.

4.2.4 Symmetry of Bases and Compact Support

Figures 4.3, 4.4 and 4.7 indicate that SA_4^b, Ort_4^b and Bmw_{12} have regular, symmetric/antisymmetric basis functions. Bmw_S bases are near-symmetric as seen in Figure 4.6. The Bmw_8 multiwavelet does not have symmetric basis functions (Figure 4.5). Strictly speaking, only SA_4^b, Ort_4^b and Bmw_{12} multiwavelets provide both symmetry and orthogonality. Due to its near-symmetric basis functions, the Bmw_S-transform may be considered orthogonal and symmetric. Thus, we expect SA_4^b, Ort_4^b, Bmw_S and Bmw_{12} to perform better than Bmw_8. We do not discuss the symmetry property for the unbalanced multiwavelets since they lack regularity for odd integer shifts.

Since all the multiwavelets are orthogonal, the synthesis filters have the same length as the corresponding analysis filters. The SA_4^u, Ort_4^u, SA_4^b, Ort_4^b and Bmw_8 multiwavelets have all 8-tap filters in the filter bank, the Bmw_{12} multiwavelet uses 12-tap filters. Bmw_S has one 8-tap and one 12-tap filter in the lowpass and highpass branches. The longer the reconstruction filters, the more pronounced are the ringing artifacts in the compressed image. So at high compression ratios we expect to see more ringing in images compressed with Bmw_{12} and Bmw_S than the other three balanced multiwavelets.

4.2.5 Symmetric Extension

As discussed in Chapter 2, the symmetric extension of the input image provides noticeable improvement in image quality. We examine this issue further for multiwavelets. As discussed in Section 2.4, we symmetrically extend a 1-D N-length input by flipping it about its border to form a $2N$-length signal. We assume that the input image dimensions are powers of two. For all of the multiwavelets under consideration, the filters have even length.

For the SA_4^u, Ort_4^u, SA_4^b, Ort_4^b, Bmw_8 and Bmw_{12} multiwavelets, the even length highpass branch filters g_0 and g_1 are both symmetric (or antisymmetric) about the same point. For symmetric filters, symmetric extension is simple; the same extension technique used for

the symmetric biorthogonal scalar wavelets (Section 2.4) is applied. When a symmetrically extended signal is input to the filter bank, the filters g_0 and g_1 each generate symmetric outputs of length $2N$. Referring to Figure 3.4, each downsampler in the highpass branch outputs $\frac{N}{2}$-length signals with even symmetry; they are interleaved to form a symmetric signal with N highpass coefficients. When its symmetric half is discarded, only $\frac{N}{2}$ highpass coefficients are retained. Thus, after one stage of decomposition of a symmetrically extended N-length signal, $\frac{N}{2}$ highpass coefficients are generated.

The lowpass branch filters h_0 and h_1 are not symmetric for these six multiwavelets; thus, these branch outputs lack symmetry. We note that h_1 is the same as h_0 flipped, i.e. h_0 and h_1 are reversed in time ($h_0(n) = h_1(l-n)$, l is the length of the FIR filter). So, for a symmetrically extended input of length N, the filter bank generates signals of length $2N$ at the output of h_0 and h_1, where, the output of h_0 is the same as the output of h_1 flipped. Therefore, the $4N$ lowpass coefficients ($2N$ at the output of both h_0 and h_1), can be fully represented by just $2N$ samples. After the downsample-by-4 operation, there are $\frac{N}{2}$ samples at the output of each of the lowpass filters. These samples are interleaved into a single N-length output; half of the output coefficients are discarded. Thus, after one stage of decomposition, an N-length input generates $\frac{N}{2}$ lowpass coefficients. This procedure is shown in Figure 4.21 for a randomly generated 16-sample input.

The Bmws is different from the other multiwavelets; its filters have linear phase but are not uniform in length. h_0 and g_0 are 8-tap while h_1 and g_1 are 12-tap. Thus the lowpass and highpass branch filters do not have a common point of symmetry. As before, if we symmetrically extend the signal while maintaining even symmetry, downsampling gives one subband with even symmetry and one with odd symmetry. Figure 4.22 illustrates the one level decomposition for Bmws using symmetric extension. In the highpass branch, if downsampling maintains even symmetry at the output of one highpass filter, the other highpass branch always generates signals with odd symmetry about a zero-valued sample (because, the symmetric input always has a zero at $f = 0.5$). The zero-valued sample is known a priori to the decoder; so, it is redundant and does not need to be encoded.

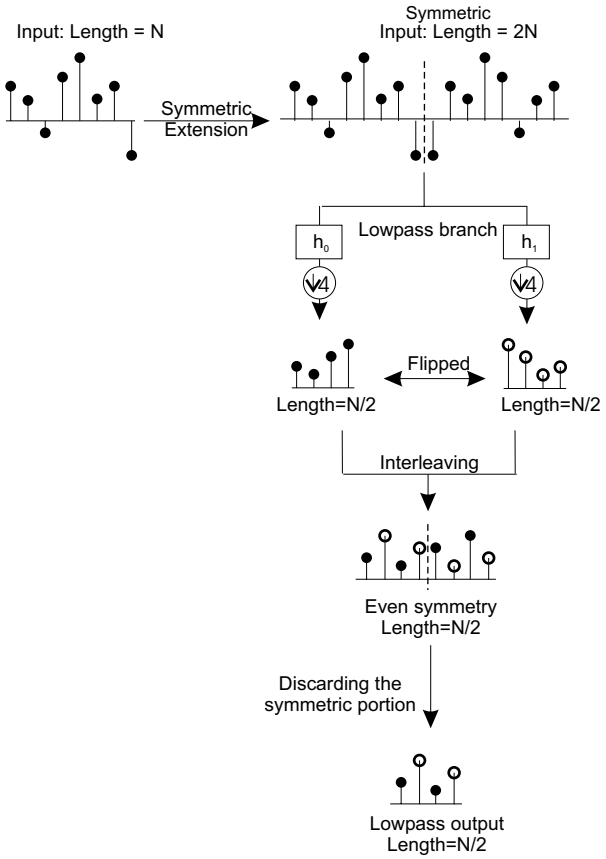

Figure 4.21: Symmetric extension for multiwavelets.

For the lowpass branch, half of the samples can be discarded from the subband with even symmetry. For the subband with odd symmetry, there is one coefficient in the subband that cannot be represented if only half of the samples are used (Figure 4.22). To overcome this problem, we send some information (such as the difference between the extra coefficient and its previous sample) about this extra lowpass coefficient in place of the redundant zero in the highpass output. We note that this technique is sub-optimal and affects the spatial prediction in the quantizer to a small extent.

Based on symmetric extension, we expect Bmw$_S$ to be at a disadvantage with respect to the other multiwavelets. In Chapter 5, we compute an upper bound on the PSNR values for Bmw$_S$ by treating its symmetric extension as an expansive technique where the extra

lowpass coefficients are encoded separately without quantization.

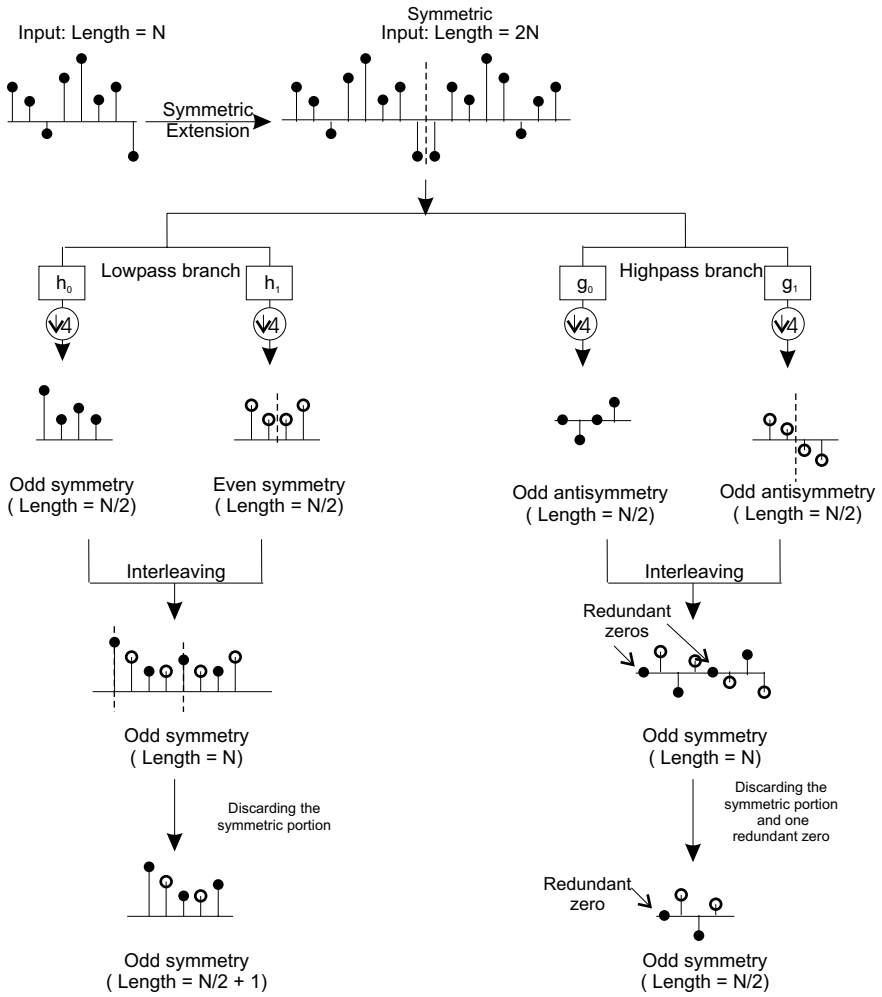

Figure 4.22: Symmetric extension for Bmws.

4.3 Summary of Filter Bank Characteristics

Table 4.2 summarizes the filter bank characteristics of the scalar wavelets and the unbalanced and balanced multiwavelets.

Table 4.2: Summary of Wavelet Characteristics.

	Scalar Wavelets			Multiwavelets						
				Unbalanced		Balanced				
	D_8	$B_{9/7}$	$B_{22/14}$	SA_4^u	Ort_4^u	SA_4^b	Ort_4^b	Bmw_8	Bmw_S	Bmw_{12}
Orthogonality	Yes	Biorthogonal		Yes		Yes				
Linear phase filters	No	Yes		No		No			Yes	No
Symmetry of basis functions	No	Yes		Not Applicable		Yes		No	Yes	
Energy compaction	Vanishing order:			Balancing order:						
	8	4,4	5,7	0	0	2	2	2	2	3
Bases under integer shifts	Shift-invariant			Shift-variant		Shift-invariant		Shift-variant	Shift-invariant	
$\phi_{i,1}(t)$, $\psi_{i,1}(t)$	Regular			Irregular		Regular				
# of zeros of $\lvert H_0(f)\rvert_{f=0.5}$	Not Applicable			0	0	2	1	0	1	0
# of zeros of $\lvert H_1(f)\rvert_{f=0.5}$				1	1	2	1	0	1	0
# of zeros of $\lvert G_0(f)\rvert_{f=0}$				1	1	2	2	2	3	0
# of zeros of $\lvert G_1(f)\rvert_{f=0}$				0	0	2	1	3	3	3
Lowpass group delay difference	Not Applicable			Not Applicable		≈ 2, $f < 0.4$	≈ 2, $f < 0.4$	≈ 2, $f < 0.3$	$= 2$, $\forall f$	≈ 2, $f < 0.35$
Compact support of filters	16	9,7	22,14	8	8	8	8	8	8,12	12
Symmetric extension	N/A	Yes		Yes		Yes			Sub-optimal	Yes